ORIGINAL ARTICLE

Antibacterial performance of GO–Ag nanocomposite prepared via ecologically safe protocols

Riya Thomas[1] · Jyothi Unnikrishnan[2] · Aparna V. Nair[1] · Elcey C. Daniel[3] · Manoj Balachandran[1]

Abstract

Control and extinction of the rising problem of antimicrobial resistance makes a multidisciplinary approach for the advancement of novel disinfectant agents imperative. Although graphene-based nanomaterials display high bacterial toxicity, their cytotoxicity to mammalian cells is found to be very low. Herein, a simple green approach for the synthesis of graphene oxide–silver composite using *Syzgium cumini* (Indian black plum) fruit extract was reported. Physicochemical properties and antibacterial activities of the composite were subsequently studied comparing with silver nanoparticles and pure graphene oxide. We demonstrate the influence of precursor materials in dictating the antibacterial properties of nanosystems. The antibacterial study conducted on selected gram-negative and gram-positive bacteria reveals that composite is more effective against gram-negative bacteria. The microbicidal activity of composite against bacteria *Pseudomonas aeruginosa and E. coli*, was higher than the control drug cephalexin (CE control). Test compounds against L929 cell lines by MTT assay reveal the low cytotoxicity of samples. From the statistical analysis, it is inferred that the cell viability is dependent on the concentration. Fruit extract-based graphene–silver composite could be an excellent environment-friendly replacement for harsh disinfectants.

Keywords Graphene–silver composite · Antibacterial activity · ESKAPE pathogens

Introduction

Growing bacterial resistance towards drugs and other disinfection agents has become a major challenge in the drug research and sanitation industry. In the past years, several pathogenic species of bacteria have undergone mutations and many have become multidrug resistant. Since most of the commonly used antibiotics have become ineffective in combating them, the development of new antibacterial agents with improved screening has become a serious apprehension among the scientific community. It is recognized from earlier investigations that, graphene nanostructures that possess sharp edges are proficient enough to rupture the bacterial cell membrane (Liu et al. 2011). Albeit, there are multiple contrary reports on the antibacterial activity of graphene derivatives. The studies of Bao et al. and Ruiz et al. revealed the absence of antibacterial activity in bare graphene oxide (GO) (Bao et al. 2011; Ruiz et al. 2011). On the other hand, many researchers detected higher antibacterial effects of GO towards several bacterial agents like *E. coli*, *Pseudomonas aeruginosa, Staphylococcus, and so on* (Hu et al. 2010; Bykkam et al. 2013). It is the variations involved in the synthesis parameters that alter the surface functional groups and size of graphene sheets which amends the biological activity of GO.

Graphenic structures embedded with inorganic nanoparticles are solitary potential candidates among other bactericidal agents and are more advantageous than the classical drugs because of their minimal cytotoxicity to mammalian cells, reduced cost, and slow development of antibacterial resistance (Ahamed et al. 2020; Madni et al. 2018). Decoration of metal nanoparticles over the graphene surface engender biological characteristics suitable for a wide range of potential uses (Upadhyay et al. 2014). Silver nanoparticles (AgNPs) that are known to be an antibacterial agent

✉ Manoj Balachandran
manoj.b@christuniversity.in

[1] Department of Physics and Electronics, CHRIST (Deemed to be University), Bengaluru, Karnataka 560029, India

[2] Department of Statistics, Kristu Jayanti College (Autonomous), Bengaluru, Karnataka 560077, India

[3] Department of Life Sciences, Kristu Jayanti College (Autonomous), Bengaluru, Karnataka 560077, India

for centuries can be utilized as an effective antimicrobial additive in the graphene–silver hybrid system. Nanoparticle aggregation that usually hinders the microbicidal properties of AgNPs can also be resolved through the formulation of nanocomposite with graphene possessing a high-specific surface area (Zhang et al. 2019). The antimicrobial effect that is a prerequisite for health, food, and pharmaceutical industries has encouraged the biological studies of the graphene–silver composite. Lei et al. prepared graphene oxide–silver nanoparticle (GO–AgNPs) composite via a direct reduction in AgNO$_3$ using NaBH$_4$ as the reducing agent (Britnell et al. 2012). Sun et al. synthesized reduced graphene oxide–silver hybrid through the chemical reduction in silver salts (Liu et al. 2010). Raynara et al. loaded the silver nanoparticles on the graphene oxide surface using electron beam irradiation (Jacovone et al. 2019). The bottlenecks associated with these conventional synthesis mechanisms comprise high cost, a great amount of energy consumption, and utilization of toxic chemicals that are hazardous to the environment.

The antibacterial efficacy of the graphene-based nanocomposites is found to be heavily dependent on precursors and the adapted synthesis route (Barbolina et al. 2016). Based on the green chemistry principles, many researchers have portrayed the synthesis of metal nanoparticles via environment-friendly procedures. Metal ions are reduced at a faster rate by plant extracts than fungi or bacteria (Makarov et al. 2014). The presence of various biomolecules, such as proteins, enzymes, amino acids, polysaccharides, alkaloids, and alcoholic compounds in plants helps in the bioreduction and stabilization of the metal nanoparticles (Kuppusamy et al. 2016). Besides, the antioxidizing agents present in plant and fruit extract, alter the layers of graphene via partial oxidation. The materials employed in biomedical applications should be stable, compatible, and biologically active. Hence, the fruit-derived silver nanoparticle is used in biomedical applications due to its biocompatibility. It is worth mentioning that the utilization of fruit extract known for pharmaceutical properties can also enhance the unparalleled biological property of silver nanoparticles. In the present study, we have used fruit extract of *Syzgium cumini* commonly known as Indian black plum to prepare GO–Ag composite. *Syzgium cumini* is a medicinal plant used for antidiabetic, antiinflammatory, antipyretic, antioxidant, and anticancer properties (Yadav et al. 2011). Therefore, the black plum extract is not only a cost-effective and plentiful source, but also a naturally available pharmaceutical agent.

To the best of our knowledge, the biocidal activity of GO–Ag nanocomposite prepared using fruit extract of *Syzgium cumini* is not described so far. Likewise, the cytotoxicity of GO–silver nanocomposites prepared via ecofriendly synthesis route towards the L929 cell line has also not been reported yet. L929 Mouse fibroblast is the most commonly

used European standards (PN-EN ISO 10993-5:2009, Polish Pharmacopeia, U.S. Pharmacopeia) for the evaluation of cytotoxicity in biological materials. Hence instead of the conventional, expensive, and ecologically unsafe protocols, the present study report facile and scalable production of highly biocidal graphene oxide–silver nanocomposites from renewable, biological substances without the aid of any hazardous chemicals or by products. The preliminary cytocompatibility screening of the GO–silver composite was carried out using in vitro evaluation of the L929 cell. The antibacterial activity of nanocomposite against both gram-positive and gram-negative bacteria was evaluated about the control drug cephalexin. In addition to this, an investigation on the antibacterial property of bare graphene oxide that persists as a debatable issue is also described. The current work integrates myriad properties of silver nanoparticles prepared using black plum extract (BA) and grapheme–silver nanocomposite (GBA) to produce highly efficient antibacterial agents that are effective under natural light.

Results and discussion

XRD analysis

The X-ray diffraction profile of graphene oxide (GO) is presented in Fig. 1a. The characteristic peak of GO due to the (002) plane is observed at $2\theta = 10.3°$ indicating its low crystallinity and amorphous structure (JCPDS File No. 41-1487) (Mututu et al. 2019). The peak at $2\theta = 42.3°$ is attributed to the defects in the graphene system. Figure 1b depicts the XRD pattern of GO–silver nanocomposite prepared using the black plum extract. The diffraction patterns of bare black plum (BB) extract show both amorphous and crystalline peaks because of the organic and inorganic biomolecules contained in the fruit. The crystalline peaks appear at $2\theta = 21°$, $24°$, $28.60°$, and $41°$ show the presence of anthocyanin compounds in BB (Favaro et al. 2018). The XRD spectrum of BA substantiates the formation of silver nanoparticles from bulk AgNO$_3$. The Bragg peaks at $2\theta = 38.62°$ (111), $46.25°$ (200), and $64.8°$ (220) are the characteristic reflection planes of Ag nanoparticle and peaks at $2\theta = 27.7°$, $32.3°$, $46.1°$, and $54.6°$ depicts the cubic phase of AgCl (JCPDS File No. 65-2871 and 31-1238) (Eya'ane Meva et al. 2016). The additional peak indicates the presence of BB extract that helps in the stabilization of nanoparticles. In the case of nanocomposite, the detected peaks at $38.2°$, $46°$, and $64.5°$ confirm the successful incorporation of Ag nanoparticle in the GO matrix (Fig. 1b). All peaks got slightly shifted to lower 2θ value and an enhancement in the peak intensity were also observed. The appearance of the characteristic peak of GO at $2\theta = 11°$ as a small spike in the composite substantiate the attachment of silver nanoparticles, inhibiting
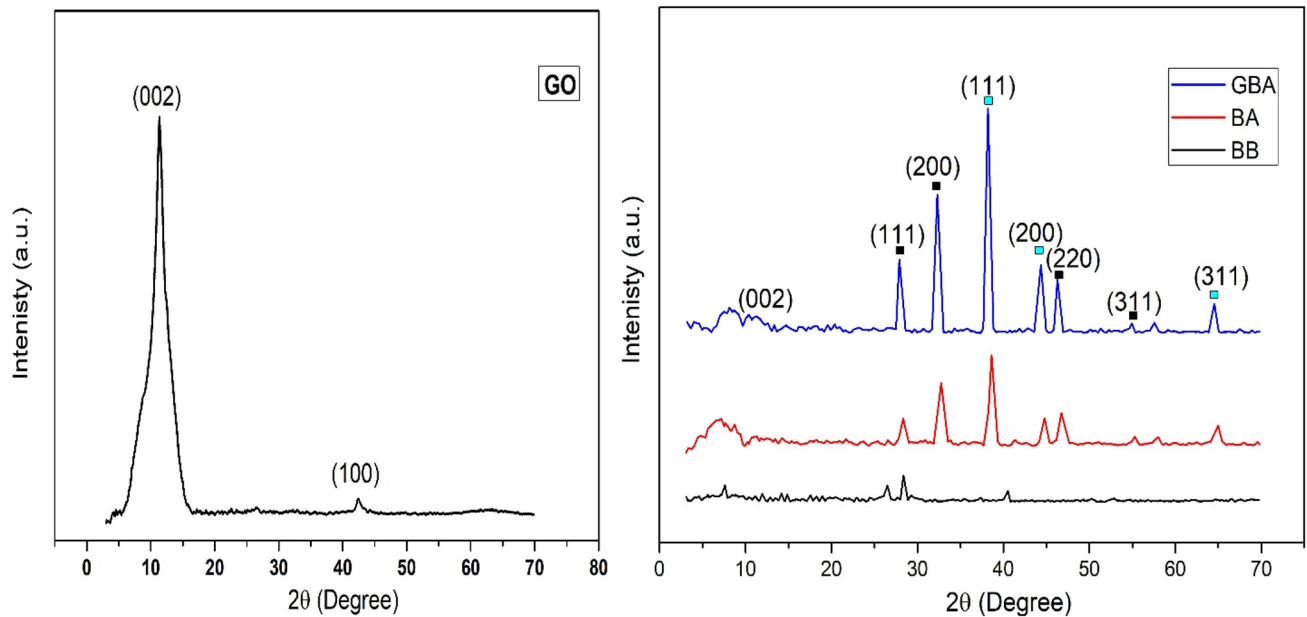
Fig. 1 XRD pattern of **a** graphene oxide (GO) **b** bare black plum (BB), silver nanoparticle (BA), graphene-oxide–silver nanocomposite (GBA) (■ represents Ag nanocrystallites, ■ represents AgCl nanocrystallites)

Table 1 Calculated interlayer spacing of silver nanoparticle (BA) and graphene oxide–silver nanocomposite (GBA)

	$d_{spacing}$ of BA (nm)	$d_{spacing}$ of GBA (nm)
(111)	2.333	2.354
(200)	1.961	1.971
(220)	1.432	1.443

the stacking of graphene layers. It is the strong reflections from Ag nanoparticles obscured the Bragg reflections from graphene planes. These observations are consistent with the earlier reports in the literature (Hareesh et al. 2016; Faria et al. 2014a).

The variation in the interlayer spacing of Ag nanoparticle on anchoring with graphene sheets is tabulated in Table 1. The calculated $d_{spacing}$ is in good agreement with standard silver values (Jyoti et al. 2016). The $d_{spacing}$ of all the planes of nanocomposite is increased as compared to pure Ag nanoparticles. This phenomenon refers to the intercalation of silver nanoparticles within the graphene surface.

FTIR analysis

The FTIR transmittance spectra provide information on the localized environment of organic molecules responsible for the reduction and stabilization of biosynthesized silver nanoparticles.

As seen in Fig. 2, the broadband observes at 3400 cm^{-1} can be indexed to alcohol, and phenol groups appeared in
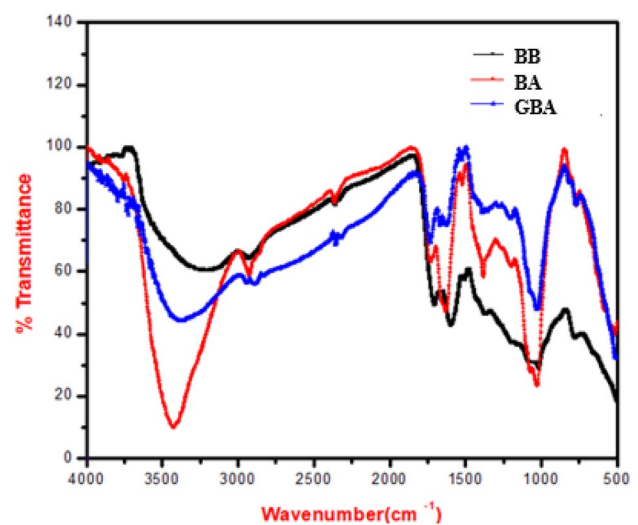

Fig. 2 FTIR spectrum of **a** bare black plum (BB), **b** silver nanoparticle (BA) **c** graphene oxide–silver nanocomposite (GBA)

association with hydroxyl compounds (O–H). The absorption bands at 3030 and 2850 cm^{-1} correspond to the C–H stretching vibration of the aromatic ring. The band at 1743 cm^{-1} exemplifies the stretching of nonconjugated C–C (Pandey and Balachandran 2020). The presence of proteins in the nanostructures can be indexed to bands at 1638 and 1043 cm^{-1} that corresponds to the stretching of C–C and C–N. Certain peaks obtained in the range of 1400–1600 cm^{-1} can be assigned to benzene skeleton vibrations. The band at 1370 cm^{-1} can be assigned to the

characteristic N=O stretching of the nitro compound. Stretching vibration of pyran rings which is typical for flavonoid compounds are observed at 1240 cm^{-1}. Bands at 980 and 735 cm^{-1} regions could be attributed to asymmetric stretching and deformation of C–H phenol ring, respectively (Espinosa-Acosta et al. 2744; Masum et al. 2019). The reduction/capping of the nanoparticles is mainly dependent on the amide linkages (N–H) of the proteins (Niraimathi et al. 2013). The absorption band corresponds to this functional group is located at 1450 cm^{-1}. These observations show that the presence and the binding of proteins with the corresponding silver nanoparticles and this may be the reason for their stabilization. The intensity of N–H stretching vibrations is found to be prominent in BA suggesting its role in the bioreduction of Ag$^+$. The evident decrement in the absorption intensity and blue shift of the peak position in GBA are clear indications of the reduction of GO on decoration with Ag nanoparticles.

Raman analysis

Raman spectra showed in Fig. 3 reveals the adsorption mechanism of biomolecules associated with the capping agents of silver nanostructures. The strong peaks observed at 850 and 1390 cm^{-1} in Fig. 3a could be assigned to the vibrational stretching of C–C and O–C–O bands; whereas the peak around 500 cm^{-1} indicates the presence of C–N–C group (Cai et al. 2017). These carboxyl and amino groups of the black plum extract are involved in the encapsulation/stabilization of Ag nanoparticles (Kora and Arunachalam 2012). The disorderliness in the graphene matrix upon intercalation with Ag nanoparticles is also analyzed using Raman spectra. Two signature D and G peaks of GO were observed around 1350 and 1600 cm^{-1}. G-band and D-band provide information on the amount of sp^2 carbon clusters and the density of involved defects respectively (Manoj 2014). After anchoring Ag nanoparticles over the surface of graphene, the graphitic band was shifted to 1590 cm^{-1} and defect band to 1380 cm^{-1}. A small downward shift of the Graphitic band
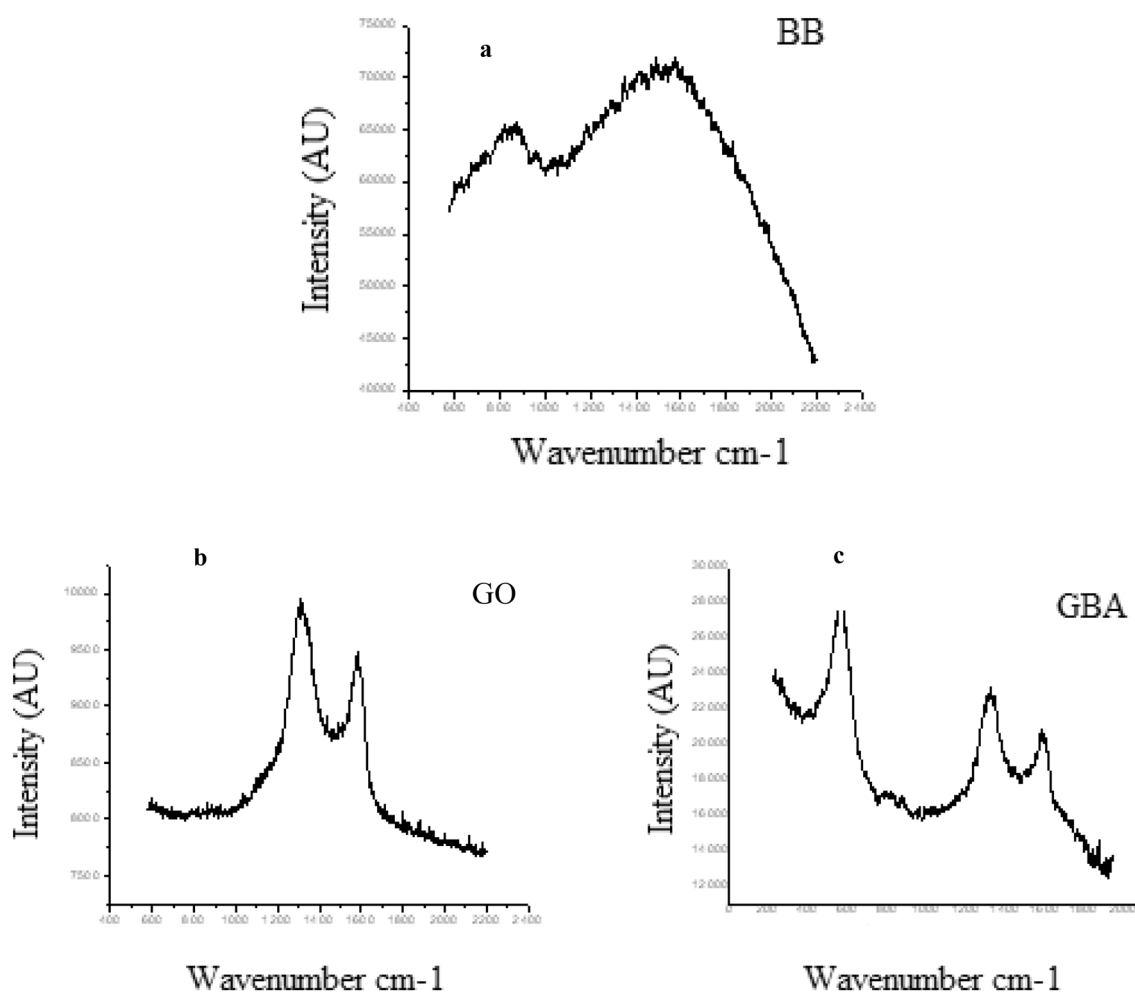

Fig. 3 Raman spectrum of **a** bare black plum (Bb) **b** graphene oxide (GO) **c** graphene oxide–silver nanocomposite (GBA)

implies the reduction of oxygen functionalities over the graphene surface due to the anchoring of nanoparticles. Interestingly, the intensities of both the bands of GBA were increased significantly, which is endorsed to the surface-enhanced Raman scattering (SERS) of Ag nanoparticles (Gurunathan et al. 2016). The additional peak appeared around 520 cm^{-1} confirms the presence of amide linkages that holding around silver nanostructures. This is favorable for the formulation of GBA as a suitable substrate for SERS activity. The intensity ratio of defect peak to graphitic peak for GO and GBA is calculated to be 1.06 and 1.08, respectively. The elevated I_D/I_G ratio of GBA emphasizes the intercalation of Ag nanoparticles within the graphene domain.

Morphological and elemental analysis

The surface morphology of the composite is investigated by TEM and is presented in Fig. 4. The image shows that silver nanoparticles of the size approximately 10–30 nm are distributed anisotropically on the surface of GO sheets. The formation of silver nanoparticles as spherical-like particles suggests the morphological influence of graphene sheets in both nucleation and stabilization processes. The GO nanostructures in the GBA composite act as morphological drivers for silver nanoparticles controlling the formation of polymorph, but highly stable nanoparticles (Shao et al. 2015). The anchoring of silver nanoparticles on the GO sheet validates the higher chemical affinity of AgNPs with oxygen species on the graphene surface. The functional group, such as –COOH, –OH provide nucleation sites for the growth of AgNPs (Pasricha et al. 2009). However, for bioderived or fruit-derived nanoparticles an additional hydrogen bonding is involved with the deposition of AgNPs over the graphene sheets. The electron pair in the amide linkages (N–H) of the

protein interact with oxygenated groups on the GO surface and hence establish an attachment of bioderived silver nanoparticles (Faria et al. 2014).

The EDS analysis shows that carbon (51.49 At wt%), oxygen (43.545 At wt%), and silver (1.87At wt%) are major elemental compositions in the nanocomposite (Fig. 5). The minor elements like Na, Mg, Si, S, Cl, and K have resulted from the black plum extract or Hummers' treatment. The formation of silver–GO composite is confirmed by the EDS analysis and is in support of X-ray and IR analysis.

Optical analysis

The optical study of synthesized nanostructures is presented in Fig. 6. The absorption maxima of BB extract at 535 nm could be attributed to the presence of a high concentration of anthocyanin derivatives (Talukder et al. 2020). Broadband
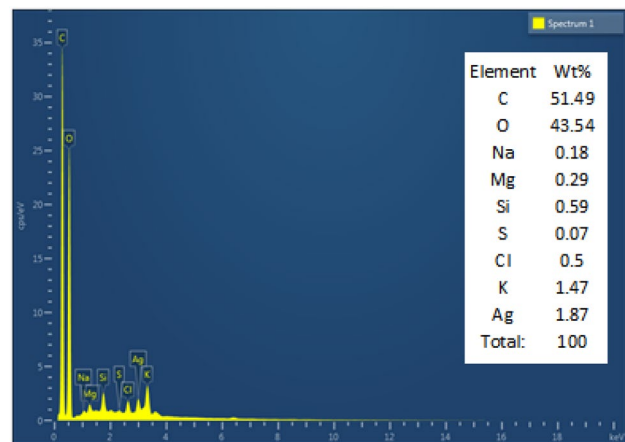

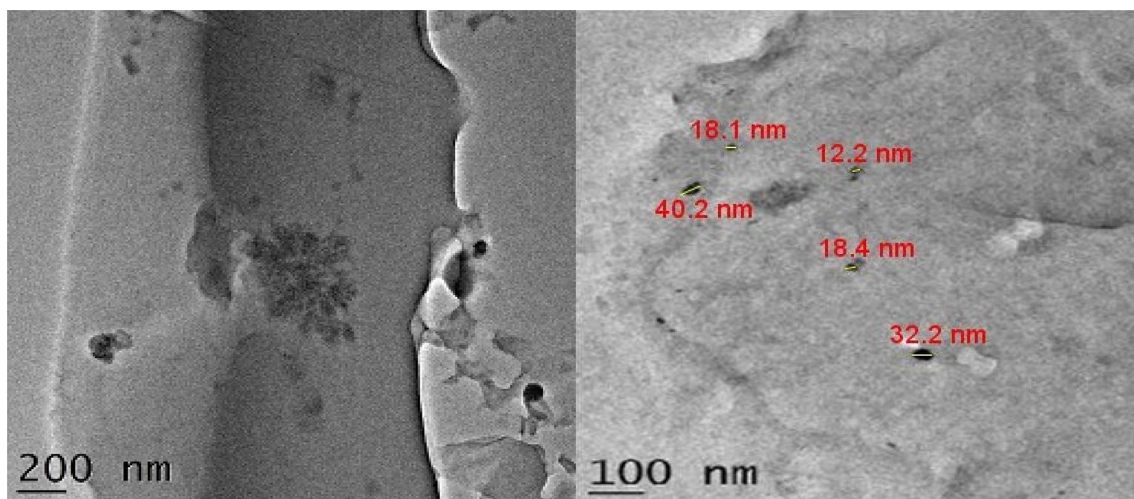**Fig. 5** EDS spectra of graphene oxide–silver nanocomposite (GBA)

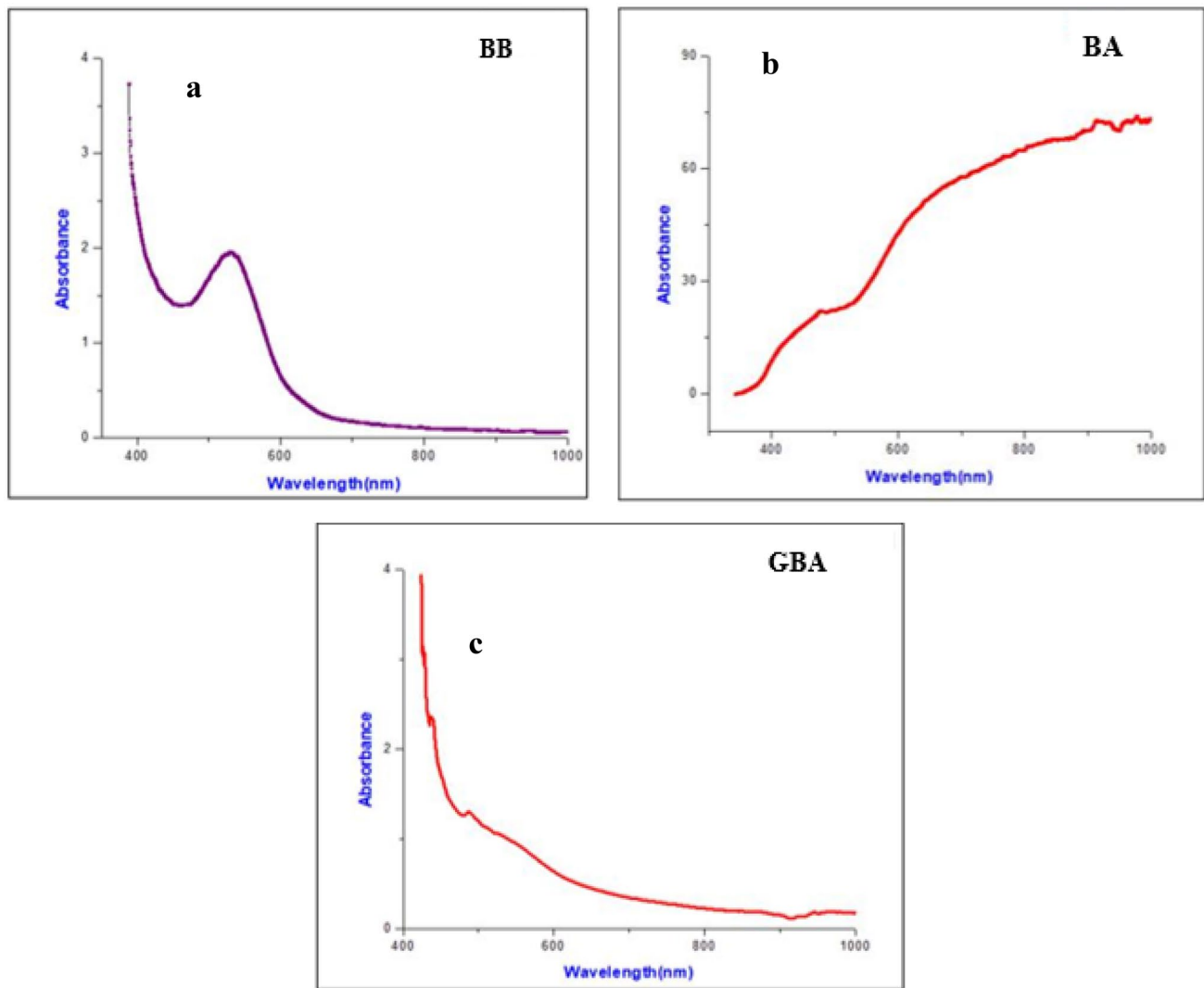**Fig. 4** TEM image of graphene oxide–silver nanocomposite (GBA)

Fig. 6 UV–Vis absorption spectra of **a** bare black plum (BB), **b** silver nanoparticle (BA) **c** graphene oxide–silver nanocomposite (GBA)

centered on 450 nm in the visible region was observed for BA. This indicates the characteristic surface Plasmon resonance peak (SPR) of the silver nanoparticles (Zafar and Zafar 2019). Although the spike observed at 500 nm indicates the presence of anthocyanin compounds. The nanocomposite GBA shows an absorption band with a decrement in the peak intensity along with a shift to a longer wavelength. This shifting is due to the formation of Ag nanoparticles with different morphology, chemical environment, and species absorbed on the surface (Huang et al. 2016). The decreasing absorption corresponds to the agglomeration of Ag nanoparticles which is also evident from TEM analysis. The SPR band in GBA confirms the occurrence of Ag nanoparticles within the composite matrix. A small spike around 410 nm is aroused from the π–π* transition of the altered electronic structure of GO upon reduction caused by the Ag nanoparticles (Khorrami et al. 2019).

The energy bandgap of the samples is obtained by plotting Tauc plot (Fig. 7) and is presented in Table 2. The GO powder obtained by modified Hummer's method has a bandgap of 2.47 eV. It is observed that by making GO–Ag composite the band gap value is increased to 2.77 eV. This shift in the energy gap is due to the reduction of oxygen functional groups over the graphene surface on interaction with Ag nanoparticles.

The fluorescence responses of the nanostructures on excitation from 300 to 350 nm are illustrated in Fig. 8. The photoluminescence spectra of BB and BA samples exhibited excitation-dependent peaks, while the spectra of GBA consist only of excitation-independent emission. PL emission is said to arise mainly from either defect states due to the presence of various functional groups or intrinsic state resulting from the recombination and quantum size effects. Emissions appearing at longer wavelengths originate from
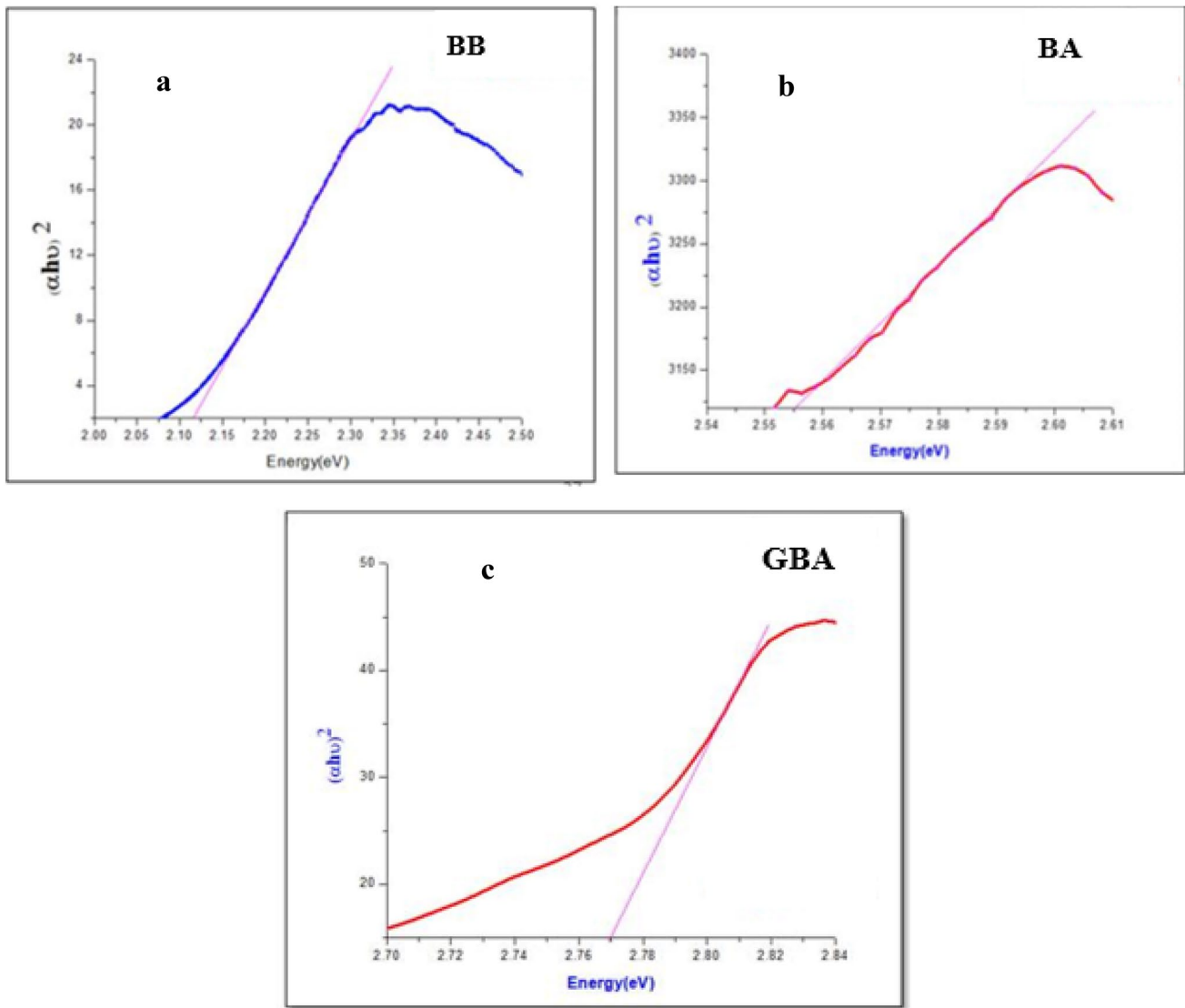
Fig. 7 Tauc plot of **a** bare black plum (BB) **b** silver nanoparticle (BA), **c** graphene oxide–silver nanocomposite (GBA)

Table 2 Determination of bandgap by Tauc plot

Compound	Energy gap in eV
BB	2.10
GO	2.47
BA	2.55
GBA	2.77

the surface energy traps whereas the emissions at shorter wavelength range are generally from intrinsic states (Manoj et al. 2018; Geim and Novoselov 2007). A combinational effect of these two could be observed in the black plum based silver nanoparticle (BA) sample. The intensity of PL emission is enhanced without any shift up to excitation wavelength of 320 nm and thereafter the emission maxima are shifted. As the excitation wavelength increases, a progressive shift in emission wavelengths is observed along with a steady rise in intensity that reaches a central maximum before declining gradually. The graphene oxide–Ag nanoparticle composite (GBA) sample exhibits more or less excitation-independent PL emission centered at 440 nm with maximum emission for 360 nm excitation wavelength. This PL-independent behavior is a direct indication of the existence of carbogenic core having a bandgap value of 2.77 eV. The absence of excitation-dependent peaks in composite spectra substantiates the reduction of oxygen moieties attached in the carbon
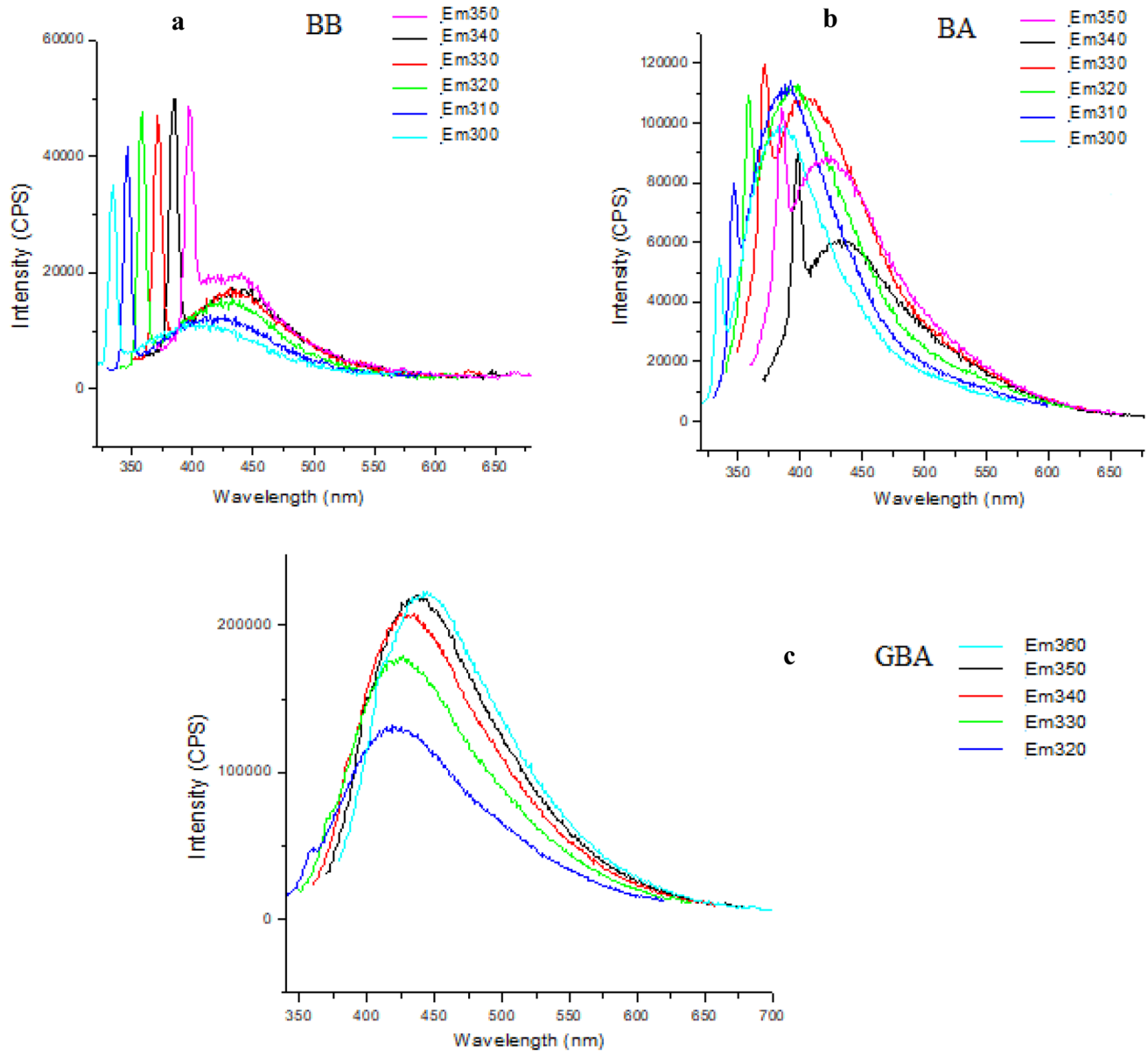
Fig. 8 Fluorescence response of **a** bare black plum extract (BB), **b** silver nanoparticle (BA), **c** graphene oxide–silver nanocomposite (GBA)

backbone. The synthesized nanomaterials possess long-term photostability and remained aggregation free for a significant duration of 18 months. This considerably enhances the commercial applicability of these materials. With tunable PL behavior and long-term stability, they might find great utility in the field of sensing and cellular imaging (Anu et al. 2019). The most frequently used nano-materials for these applications are silver nanoparticles which are toxic, expensive, and lack good photostability (Liu et al. 2015). Hence, the use of bioderived nano-composite as a low cost and viable alternative for these

applications appears promising and needs to be explored further.

Cytotoxicity studies

The synthesized samples show evidence of different physicochemical properties. Proper understanding of the surface chemistry of graphene on decoration with Ag nanoparticles towards the response of living cells is also of vital importance. To corroborate these findings, cytotoxicity properties of BA and GBA are evaluated and compared with GO sheets. To assess the cytotoxicity of the synthesized nanocomposite,

Fig. 9 Viability of L929 cell lines after 72-h exposure to 100–1000 μg/mL of graphene oxide (GO), black plum-oxidized silver nanoparticle (BA) and graphene oxide–silver nanoparticle composite (GBA) (triplicate incubation for the three treatment was conducted for five different concentation. Comparison of cytotoxicity of the nanomaterials after 72 h exposure is presented in the figure)

Effect of Nanostructure on Viability of L929 Cell lines
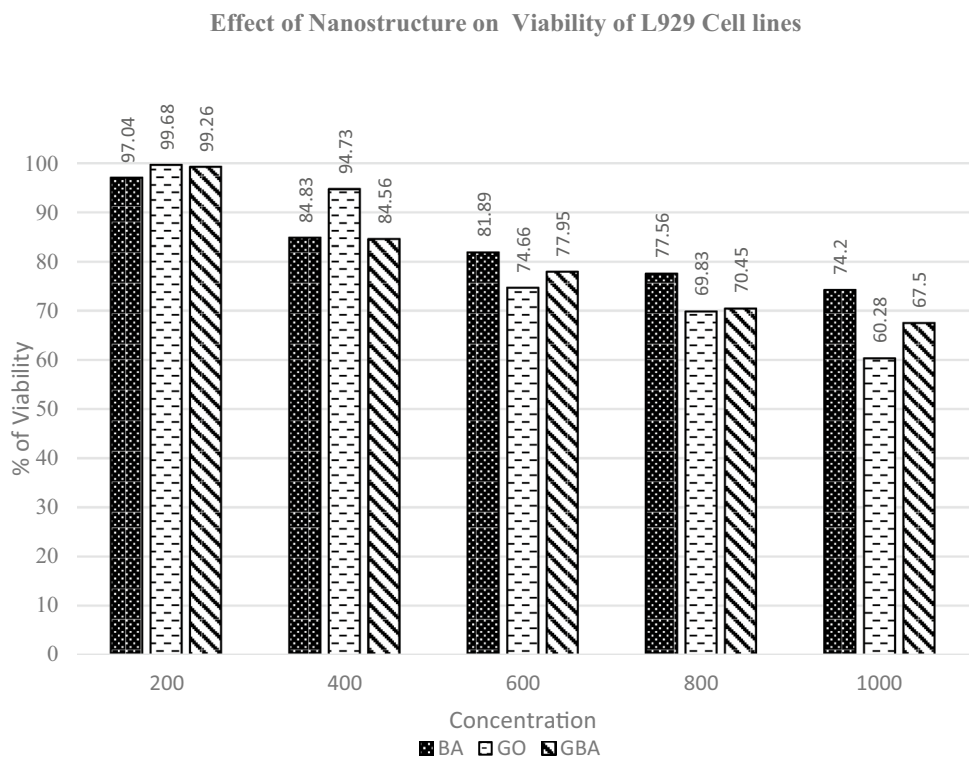
the toxic activity of the compounds against L929 cell lines was evaluated over 24 h using the MTT colorimetric assay. The effect of the concentration of the nanostructure on viability (% of L929 cell lines) is presented in Fig. 9. There is a significant reduction in the cells' survival in all three samples. The sample BA and GBA show greater reduction until 400 μg/mL. The GO sample shows a maximum reduction in cell viability of about 40% at a concentration of 1000 μg/mL whereas GBA exhibits 32.2% and BA shows a ~ 25% reduction in the viability for the same concentration. Pure GO and GO–Ag composite (GBA) exhibit higher levels of cytotoxicity, since they reduce the viability of cell by 40% and 32.2% in 24 h. It is interesting to notice that GO is exhibiting higher toxicity against the treated cells for the studied concentration and time. The composite GBA is showing moderate cytotoxicity towards the L929 cell line. This decreased toxicity of composite in comparison to bare GO can be attributed to the better intercalation of silver nanoparticles and the formation of a stable complex with GO (Cobos et al. 2020). However, there are many reports on the increased cytotoxic property of GO–Ag composite than their pristine counterparts (Wierzbicki et al. 2019). The vital parameter which determines the toxicity of nanocomposite is the dose of nanohybrid, i.e., the mass ratio of GO:Ag. Herein, we could derive a GO–silver hybrid system with improved viability towards living cells.

It is worthwhilw to point that the change in concentration is causing variation in the viability. Noticeable lowering of viability is observed at the concentration of 600 μg/mL when compared with 200 and 400 μg/mL. To test and prove statistically whether this difference is significant, the analysis of variance is carried out. The null hypothesis for ANOVA test is that the five samples do not differ in the average viability due to change in concentration. The test result is presented in Table 3

The F statistic value is 20.331 with a significance value < 0.01, hence the null hypothesis is rejected at 1% level of significance. Therefore, with 99% confidence, it can be inferred that the sample means differ significantly between the 5 concentration. Furthermore, to comprehend which of the concentrations really differ, post hoc analysis using Bon Ferroni test is carried out (Table 4).

The null hypothesis is the pairs do not differ significantly in the average viability due to difference in concentration. The significance value < 0.05 infers rejection of the null hypothesis at 5% level. From the results, we can comment that there is enough sample evidence to conclude that the

Table 3 Output table of ANOVA test

Source of variation	Sum of squares	df	Mean square	F	Sig
Concentration	1880.094	4	470.024	20.331	0.000**
Error	231.184	10	23.118		
Total	2111.278	14			

**Significant at 1% level

Table 4 Post hoc tests by Bonferonni for multiple comparison

(I) Concentration (µg/mL)	(J) Concentration (µg/mL)	Mean difference (I–J)	Std. error	Sig
200	400	10.62	3.92584	0.221
	600	20.49	3.92584	0.004**
	800	26.04	3.92584	0.001**
	1000	31.33	3.92584	0.000**
400	600	9.873	3.92584	0.307
	800	15.42	3.92584	0.028*
	1000	20.71	3.92584	0.004**
600	800	5.550	3.92584	1.000
	1000	10.84	3.92584	0.201
800	1000	5.29000	3.92584	1.000

** and *Significant at 1% level and 5%, respectively

viability of concentration 200 µg/mL is significantly different from 600, 800, to 1000 µg/mL. However, concentration 400 µg/mL is different from 200, 800, and 1000 µg/mL. The concentrations 800 and 1000 µg/mL do not differ significantly in the average viability. However, the three samples (BA, GO, and GBA) do not differ in the average viability for a given concentration (ANOVA test, $F = 0.1$ with significance $= 0.906 > 0.05$).

MIC analysis

The quantitative determination of the antibacterial activity of the nanostructures is carried out employing MIC assay using agar dilution method against two gram-negative bacteria (*E. coli and Pseudomonas aeruginosa*) and two gram-positive bacteria (*Bacillus sp. and Staphylococcus sp.*). In this method, graded amounts of the samples were added to nutrient agar plates and incubated with the organisms under study. Bacterial growth was observed as the concentration of the samples in the agar plate diminishes. The inhibition of growth at the minimum or lowest concentration of the sample was regarded as the minimum inhibiting concentration (MIC) (Ruangpan 2004). The results of the MIC assay are summarized in Table 5. GO, BA, and GBA of concentration 1 mg, 2 mg, and 4 mg are treated with gram-negative and

positive bacteria. The analysis shows that the sample BA is effective against both gram-positive and gram-negative bacteria. In the present study, 1 mg of the BA sample was effective against the *E. coli* and *Pseudomonas aeruginosa*. On adding fruit-derived silver nanoparticle to graphene oxide, the antibacterial property of the composite against the gram-positive bacteria is not appreciable, whereas the structure effectively resists the growth of gram-negative bacteria, *E. coli* and *P. aeruginosa*. This variation in the diameter of the zone of inhibition is owing to the distinction in the susceptibility of nanocomposite against different bacteria (Shao et al. 2015). The gram-positive bacteria possess a thick peptidoglycan layer that is 4–5 times thicker than that of gram-negative bacteria (Silhavy et al. 2010). Techoic acid and lepotechoice acid, which are unique to the gram-positive cell wall also might help in imparting resistance to the organisms.

The complete mechanism involved in the antibacterial action of GO–Ag nanocomposite remains uncertain. The most possible mechanisms are the synergistic effects of the GO–silver hybrid system and the higher stability of nanostructures. Xu et al. (2011) have termed this process of antibacterial action as the "Capturing-killing process". The GO sheet facilitates the formation of a hydrogen bond between the oxygen functional group on GO and lipopolysaccharides in the bacterial cell membrane. This benefits the deposition of bacteria over the GO surface through improved interaction with silver nanoparticles. The reactive oxygen species (ROS) produced by these AgNPs generate oxidative stress in the cellular surface leading to bacterial cell death. The surface nanoparticles are oxidized to form Ag^+ ions in the presence of dissolved oxygen in the aqueous media. These ions can interfere with sulfur-containing proteins, such as thiol, responsible for enzymatic activity, and can cause irreversible damage to the phosphorus-containing compounds in DNA (Cobos et al. 2020). The enhanced antibacterial activity of the fruit-derived silver nanoparticles could be attributed to direct exposure to bacterial cells. In the present study, it is worthwhile to mention that GO was not effective against the studied bacteria. The conflicting antibacterial activity of GO observed from the studies accomplished until now, in suspension can be ascribed to the factors, such as thickness and

Table 5 Diameter of inhibition zone (DIZ—in mm) and MIC (mg/mL) of synthesized graphene oxide (GO), silver nanoparticle (BA), and graphene oxide–silver nanoparticle composite (GBA) against different bacterial species

ORGANISM	GO			BA			GBA		
	1 mg	2 mg	4 mg	1 mg (mm)	2 mg (mm)	4 mg (mm)	1 mg (mm)	2 mg (mm)	4 mg (mm)
E. coli	–	–	–	10	10	14	10	11	12
Bacillus	–	–	–	~8	10	12	–	–	–
staphylococcus	–	–	–	–	~6	10	–	–	–
Pseudomonas aeruginosa	–	–	–	11	13	14	~4	~7	10

size of the graphene sheet, surface area, surface roughness, degree of oxidation, and so on (Faria et al. 2014). The antibacterial bacterial activity of GO against the gram-positive microorganism is found to be low compared to BA. Because it is the synergistic interaction between GO and Ag nanoparticle imparting bacterial toxicity, the no antibacterial effect of the pristine GO effectively lowers the antibacterial activity of the composite considerably. The synergistic effect of components in a hybrid system is to enhance the biological activity; however, it might also reduce or extinguish this activity (Soto et al. 2005).

Since the composite GBA exhibited higher antibacterial activity against gram-negative bacteria, the inhibitory effect is further investigated at lower concentrations (Table 6). The antibiotic Cephalexin was used a positive control and as a negative control, wells containing only the cells were used. Dimethyl sulfoxide (DMSO) was used for the dissolution of the tested compounds. The microbicidal activity was tested against bacteria *Pseudomonas aeruginosa and E. coli*, both samples exhibited higher activity than the control drug cephalexin (CE control). This result is promising among plant-based GO–Ag nanosystems. The antibacterial activity study is planning to extend to other ESKAPE pathogens as future work (Mohan and Manoj 2020; Manoj and Mohan Anu 2019).

Conclusion

Concerns surrounding use of antibiotic, including environmental hazards and the appearance of multidrug bacteria, can be minimized by designing antibiotics that are specific to each species of pathogen, instead of using broad-range antibiotics that are prevalent. The present study reports the synthesis of graphene–silver nanocomposite with the aid of Indian black plum extract. From the MIC analysis, it is observed that the composite has higher antimicrobial efficacy towards gram-negative bacteria in comparison to gram-positive bacteria. At lower concentrations, the antibacterial activity of composites against gram-negative bacteria was higher than that of control drug cephalexin. The synthesized GO was found to be nontoxic against gram-positive and negative bacteria. The composite GBA is showing moderate

cytotoxicity towards the L929 cell line by MTT assay when tested with various concentrations of cells. This highly effective fruit-based nanomaterial with its high viability and antimicrobial activity can be an economically viable and eco-friendly disinfectant. It can considerably lower the risk due to the overdosage of commonly used antimicrobial chemicals against the bacterial strains.

Experimental part

All the reagents used in the present study were analytical grade and were used without further purification. The chemical reagents were of high purity (graphite powder, silver nitrate (99.98%), hydrogen peroxide (30%), hydrochloric acid (37%), and potassium permanganate (99.0%)). Standard bacterial strains of *Escherichia coli* (35,218 ATCC), *Pseudomonas aeruginosa* (1214PTCC), Staphylococcus aureus (1289 ATCC), Bacillus sp. and L929 cell lines were used for the present analysis.

Graphite powder (3 g) was added to 70 ml H_2SO_4 (98%), with continuous stirring in an ice bath for 1 h. $KMnO_4$ (9 g) was added to the above mixture slowly within half an hour while maintaining the temperature at 20 °C for 2 h. The sample then kept at 40 °C in an oil bath with vigorous stirring for 30 min. Deionized water (150 mL) was added within 10 min with further stirring for 15 min at 95 °C followed by the addition of 500 mL of deionized water and 15 mL H_2O_2 (30%). Further filtration and washing with 1:10 aqueous solution of HCl (250 mL) are carried out with an addition of 600 mL deionized water. The sample was kept for dialysis for 1 week.1.2 L of deionized water is added and kept for overnight stirring followed by sonication for 30 min. Finally, the sample is separated by centrifugation at 10,000 rpm for 45 min and dried in vacuum (GO).

Indian black plum (250 g) is collected, weighed, washed, and kept in a cool place. 5 L of water is added to it and heated until the quantity is reduced to 1 L. The extract is filtered to obtain the bare black plum (BB) extract. BB extract (50 mL) is added to a beaker with 20 mL deionized water and kept for stirring for 30 min at 60 °C.1 mL Silver nitrate is added and stirred for 30 min the mixture was further centrifuged at 3000 rpm for 15 min. The sample is dried in a

Table 6 Diameter of inhibition zone (DIZ—in mm) and MIC (μg/mL) of synthesized graphene oxide (GO), silver nanoparticle (BA), and graphene oxide–silver nanoparticle composite (GBA) against gram negative bacteria

Sample	*Pseudomonas aeruginosa*				*E. coli*			
	Sample concentration in μg				Sample Concentration in μg			
	100 μg	200 μg	300 μg	400 μg	100 μg	200 μg	300 μg	400 μg
GBA	8	10	12	13	10	12	13	15
BA	7	8	9	12	8	10	11	13
CE	6	6	9	12	6	8	10	12

vacuum oven at 100 °C to obtain sample BA. In another approach, BB extract (50 mL) is added to a beaker with 20 mL deionized water and stirred for 30 min at 60 °C. To this mixture, silver nitrate (1 mL) is added and kept for stirring for 30 min. GO (5 mg) is added to 10 mL of deionized water and kept for ultrasonication for 1 h and mixed with the obtained BB extract and silver nitrate solution. The final product is vacuum dried at 100 °C to obtain an Ag–GO composite (GBA).

The X-ray diffraction (XRD) profile was recorded using Bruker AXS D8 Advance Diffractometer having Cu-radiation source of wavelength 1.5406 Å. Fourier-transform infrared (FTIR) spectra were obtained Shimadzu-FT-IR-8400 spectrometer (KBr beam splitter). Raman spectra were studied using Horiba LABRAM-HR (514.5 nm, CCD detector) spectrometer. Elemental composition was investigated with the help of energy-dispersive X-ray spectroscopy (Carl Zeiss AG ULTRA 55). The morphological analysis of the samples was performed in high-resolution transmission electron microscope (HR-TEM) (Jeol/JEM 2100). UV–Vis spectroscopy (Ocean optics) was used to assess the absorption spectra and energy gap of the material. Photoluminescence (PL) spectra of the samples were examined via Shimadzu Spectrofluorophotometer (RF5301PC).

In this study, the synthesized products namely BA, GO, and GBA was tested for its cytotoxicity on the mouse fibroblast cell line (L929) with concentrations of the compound that were set as 100 to 1000 μG/mL. Minimum inhibitory concentration (MIC) assay of the nanostructures was carried out using the microdilution plate method with resazurin. MIC assay of the synthesized nanostructures was tested against clinically isolated gram-negative bacteria (*P. aeruginosa* and *E. coli*) and gram-positive bacteria (*Bacillus and Staphylococcus*). All the experiments were conducted in triplicate to minimize the errors. The quantitative determination of the antibacterial activity of the synthesized samples is carried out employing MIC assay using agar dilution method against *E. coli*, *Pseudomonas aeruginosa*, *Bacillus sp*., and *Staphylococcus sp.*

Author contributions RT: synthesis of composite, characterization, data curation, writing—original draft, and visualization. JU: statistical analysis, interpretation and design of statstical tools for antibacterial studies. Language editing of the final proof. AVN: recording and analysis of X-ray profile, IR, and UV spectroscopic studies. Assisted in synthesis of GO, analysis of the results, and data interpretation. ECD: execution of antibacterial analysis and toxicity studies of the sample. MB: conceptualization, methodology, validation, resources, writing—review and editing, supervision, and project administration.

Compliance with ethical standards

References

Ahamed M, Akhtar MJ, Khan MA (2020) Investigation of cytotoxicity, apoptosis, and oxidative stress response of Fe3O4-RGO nanocomposites in human liver HepG2 cells. Materials 13(3):660

Anu N, Mohan MB, Panicker S (2019) Facile synthesis of graphene–tin oxide nanocomposite derived from agricultural waste for enhanced antibacterial activity against *Pseudomonas aeruginosa*. Sci Rep 9:4170

Bao Q, Zhang D, Qi P (2011) Synthesis and characterization of silver nanoparticle and graphene oxide nanosheet composites as a bactericidal agent for water disinfection. J Colloid Interface Sci 360:463–470

Barbolina I, Woods CR, Lozano N, Kostarelos K, Novoselov KS, Roberts IS (2016) Purity of graphene oxide determines its antibacterial activity. 2D Materials 3:025025

Britnell L, Gorbachev RV, Jalil R, Belle BD, Schedin F, Mishchenko A, Georgiou T, Katsnelson MI, Eaves L, Morozov SV, Peres NM (2012) Field-effect tunneling transistor based on vertical graphene heterostructures. Science 335:947–950

Bykkam S, Rao K, Chakra C, Thunugunta T (2013) Synthesis and characterization of graphene oxide and its antimicrobial activity against klebseilla and staphylococus. Int J Adv Biotechnol Res 4:142

Cai Y, Piao X, Gao W, Zhang Z, Nie E, Sun Z (2017) Large-scale and facile synthesis of silver nanoparticles via a microwave method for a conductive pen. RSC Adv 7:34041–34048

Cobos M, De-La-Pinta I, Quindós G, Fernández MJ, Fernández MD (2020) Graphene oxide–silver nanoparticle nanohybrids: synthesis, characterization, and antimicrobial properties. Nanomaterials 10:376

de Faria AF, de Moraes AC, Marcato PD, Martinez DS, Durán N, Souza Filho AG, Brandelli A, Alves OL (2014) Eco-friendly decoration of graphene oxide with biogenic silver nanoparticles: antibacterial and antibiofilm activity. J Nanopart Res 16:2110

De Faria AF, Martinez DST, Meira SMM (2014a) Anti-adhesion and antibacterial activity of silver nanoparticles supported on graphene oxide sheets. Colloids Surf B Biointerfaces 113:115–124

Espinosa-Acosta G, Ramos-Jacques AL, Molina GA, Maya-Cornejo J, Esparza R, Hernandez-Martinez AR, Sánchez-Gonzalez I, Estevez M (2018) Stability analysis of anthocyanins using alcoholic extracts from black carrot (*Daucuscarota* ssp. Sativus var. *Atrorubens* Alef.). Molecules 23(11):2744

Eya'ane Meva F, Segnou ML, Ebongue CO, Ntoumba AA, Kedi PB, Deli V, Etoh MA, Mpondo EM (2016) Spectroscopic synthetic optimizations monitoring of silver nanoparticles formation from Megaphrynium macrostachyum leaf extract. Revista Brasileira de Farmacognosia 5:640–646

Favaro LI, Balcao VM, Rocha LK, Silva EC, Oliveira JM Jr, Vila MM, Tubino M (2018) Physicochemical characterization of a crude anthocyanin extract from the fruits of Jussara (Euterpe edulisMartius): potential for food and pharmaceutical applications. J Braz Chem Soc 29:2072–2088

Geim AK, Novoselov KS (2007) The rise of graphene. Nat Mater 6(3):183–191

Gurunathan S, Hyun Park J, Choi YJ, Woong Han J, Kim JH (2016) Synthesis of graphene oxide-silver nanoparticle nanocomposites: an efficient novel antibacterial agent. Curr Nanosci 12:762–773

Hareesh K, Williams JF, Dhole NA, Kodam KM, Bhoraskar VN, Dhole SD (2016) Bio-green synthesis of Ag–GO, Au–GO and Ag–Au–GO nanocomposites using Azadirachtaindica: its application in SERS and cell viability. Mater Res Express 3:075010

Hu W, Peng C, Luo W, Lv M, Li X, Huang Q (2010) Graphene-based antibacterial paper. ACS Nano 4:4317–4323

Huang L, Yang H, Zhang Y, Xiao W (2016) Study on synthesis and antibacterial properties of Ag NPs/GO nanocomposites. J Nanomater 2016:5685967

Jacovone RM, Soares JJ, Sousa TS, Silva FR, Garcia RH, Nguyen HN, Rodrigues DF, Sakata SK (2019) Antibacterial activity of silver/reduced graphene oxide nanocomposite synthesized by sustainable process. Energy Ecol Environ 4:318–324

Jyoti K, Baunthiyal M, Singh A (2016) Characterization of silver nanoparticles synthesized using Urticadioica Linn. leaves and their synergistic effects with antibiotics. J Radiat Res Appl Sci 9:217–227

Khorrami S, Abdollahi Z, Eshaghi G, Khosravi A, Bidram E, Zarrabi A (2019) An improved method for fabrication of Ag-GO nanocomposite with controlled anti-cancer and anti-bacterial behavior; a comparative study. Sci Rep 9:1

Kora AJ, Arunachalam J (2012) Green fabrication of silver nanoparticles by gum tragacanth (Astragalusgummifer): a dual functional reductant and stabilizer. J Nanomater 2012:869765

Kuppusamy P, Yusoff MM, Maniam GP, Govindan N (2016) Biosynthesis of metallic nanoparticles using plant derivatives and their new avenues in pharmacological applications—an updated report. Saudi Pharm J 24:473–484

Liu S, Tian J, Wang L, Li H, Zhang Y, Sun X (2010) Stable aqueous dispersion of graphene nanosheets: noncovalent functionalization by a polymeric reducing agent and their subsequent decoration with Ag nanoparticles for enzymeless hydrogen peroxide detection. Macromolecules 43:10078–10083

Liu S, Zeng TH, Hofmann M, Burcombe E, Wei J, Jiang R, Kong J, Chen Y (2011) Antibacterial activity of graphite, graphite oxide, graphene oxide, and reduced graphene oxide: membrane and oxidative stress. ACS Nano 5:6971–6980

Liu L, Liu J, Wang Y, Yan X, Sun DD (2015) Facile synthesis of monodispersed silver nanoparticles on graphene oxide sheets with enhanced antibacterial activity. J Compos Mater 49:2329–2335

Madni A, Noreen S, Maqbool I, Rehman F, Batool A, Kashif PM, Rehman M, Tahir N, Khan MI (2018) Graphene-based nanocomposites: synthesis and their theranostic applications. J Drug Target 26(10):858–883

Makarov VV, Love AJ, Sinitsyna OV, Makarova SS, Yaminsky IV, Taliansky ME, Kalinina NO (2014) "Green" nanotechnologies: synthesis of metal nanoparticles using plants. Acta Naturae (англоязычнаяверсия) 6:35–44

Manoj B (2014) Systematic investigations of graphene layers in subbituminous coal. Russ J Appl Chem 87:1726–1733

Manoj B, Mohan Anu N (2019) Antibacterial composition against pseudomonas aeruginosa and method of preparation thereof, Temp/e1/46606/2019che, 201941043986a

Manoj B, Ashlin MR, George CT (2018) Tailoring of low-grade coal to fluorescent nanocarbon structures and their potential as a glucose sensor. Sci Rep 8:13891

Masum MM, Siddiqa MM, Ali KA, Zhang Y, Abdallah Y, Ibrahim E, Qiu W, Yan C, Li B (2019) Biogenic synthesis of silver nanoparticles using Phyllanthusemblica fruit extract and its inhibitory action against the pathogen Acidovoraxoryzae Strain RS-2 of rice bacterial brown stripe. Front Microbiol 10:820

Mohan A, Manoj B (2020) Extraction of graphene nanostructures from *Colocasia esculenta* and *Nelumbo nucifera* leaves and surface functionalization with tin oxide: evaluation of their antibacterial properties. Chem Eur J 26(36):8105–8114

Mututu V, Sunitha AK, Thomas R, Pandey M, Balachandran M (2019) An investigation on structural, electrical and optical properties of GO/ZnO nanocomposite. Int J Electrochem Sci 14:3752–3763

Niraimathi KL, Sudha V, Lavanya R, Brindha P (2013) Biosynthesis of silver nanoparticles using *Alternanthera sessilis* (Linn.) extract and their antimicrobial, antioxidant activities. Colloids Surf B Biointerfaces 102:288e291

Pandey M, Balachandran M (2020) Flexible polymer composite films incorporated with Li-ion/reduced graphene oxide: excellent optical and photoluminescence performance. Appl Nanosci 10:401–410

Pasricha R, Gupta S, Srivastava A (2009) A facile and novel synthesis of Ag–graphene-based nanocomposites. Small 20:2253–2259

Ruangpan L (2004) Minimal inhibitory concentration (MIC) test and determination of antimicrobial resistant bacteria. In: Laboratory manual of standardized methods for antimicrobial sensitivity tests for bacteria isolated from aquatic animals and environment, pp 31–55.

Ruiz ON, Fernando KS, Wang B, Brown NA, Luo PG, McNamara ND, Vangsness M, Sun YP, Bunker CE (2011) Graphene oxide: a nonspecific enhancer of cellular growth. ACS Nano 5:8100–8107

Shao W, Liu X, Min H, Dong G, Feng Q, Zuo S (2015) Preparation, characterization, and antibacterial activity of silver nanoparticle-decorated graphene oxide nanocomposite. ACS Appl Mater Interfaces 7:6966–6973

Silhavy TJ, Kahne D, Walker S (2010) The bacterial cell envelope. Cold Spring Harb Perspect Biol 2:000414

Soto KF, Carrasco A, Powell TG, Garza KM, Murr LE (2005) Comparative in vitro cytotoxicity assessment of some manufactured nanoparticulate materials characterized by transmission electron microscopy. J Nanopart Res 7:145–169

Talukder S, Mendiratta SK, Kumar RR, Agrawal RK, Soni A, Luke A, Chand S (2020) Jamun fruit (Syzgiumcumini) skin extract based indicator for monitoring chicken patties quality during storage. J Food Sci Technol 57:537–548

Upadhyay RK, Soin N, Roy SS (2014) Role of graphene/metal oxide composites as photocatalysts, adsorbents and disinfectants in water treatment: a review. RSC Adv 4:3823–3851

Wierzbicki M, Jaworski S, Sawosz E, Jung A, Gielerak G, Jaremek H, Łojkowski W, Woźniak B, Stobiński L, Małolepszy A, Chwalibog A (2019) Graphene oxide in a composite with silver nanoparticles reduces the fibroblast and endothelial cell cytotoxicity of an antibacterial nanoplatform. Nanoscale Res Lett 14:1–1

Xu WP, Zhang LC, Li JP, Lu Y, Li HH, Ma YN, Wang WD, Yu SH (2011) Facile synthesis of silver@ graphene oxide nanocomposites and their enhanced antibacterial properties. J Mater Chem 21:4593–4597

Yadav SS, Meshram GA, Shinde D, Patil RC, Manohar SM, Upadhye MV (2011) Antibacterial and anticancer activity of bioactive fraction of *Syzygiumcumini* L. seeds. HAYATI J Biosci 18:118–122

Zafar S, Zafar A (2019) Biosynthesis and characterization of silver nanoparticles using phoenix dactylifera fruits extract and their in vitro antimicrobial and cytotoxic effects. Open Biotechnol J 13:37–46

Zhang H, Liu W, Yang L, Liu J, Wang Y, Mao X, Wang J, Xu X (2019) Fabrication of reduced graphene oxide-Ag nanocomposites and analysis on the interaction with BSA. J Nanomater 2019:2707909